Modeling and Control of a Fixed-Wing High-Speed Mini-UAV

Mesut Bilici[1]*, Mehmet Karalı[2]

[1] *Necmettin Erbakan University, Faculty of Aviation and Space Sciences, İstanbul, Turkiye*
    mbilici@erbakan.edu.tr - 0000-0002-0016-1600

[1] *Necmettin Erbakan University, Faculty of Engineering, İstanbul, Turkiye*
    mkarali@erbakan.edu.tr - 0000-0002-2380-0575

Abstract

High-speed Unmanned Aerial Vehicles (UAVs) will be an interesting subject of study in today's aviation technology because of their ingenuity in obtaining high speeds while maintaining good maneuverability. In this study, modeling and control of a fixed-wing high-speed mini-UAV are performed. Aerodynamic analyses of the vehicle with a wingspan of 1.2 meters and a total take-off weight of 1.1 kg are done with the help of some computational fluid dynamics software. A developed MATLAB/Simulink code evaluates flight performance after a doublet control surface disturbance with six-degrees-of-freedom flight simulations in both longitudinal and lateral directions by a developed MATLAB/Simulink code. The transfer functions are obtained by trimming the aircraft at wing-level for a speed of 155 km/h, and the maximum speed that the mini-UAV could reach is calculated as 400 km/h. Two kinds of different linear controllers are designed to hold the pitch angle of the vehicle to the desired value. The time responses of the controllers are represented, and the elevator deflection effort is evaluated. Finally, a compulsive pitch angle is wanted to be tracked by the two controllers, and their responses are compared in terms of performance and stability.

1. Introduction

Unmanned aerial vehicles (UAVs) have made significant development in both study and application over the last few decades because they replaced manned aircraft in a variety of crucial and precarious operations. For the time being, the two most common types of mini-UAV platforms are fixed-wing conventional aircraft and Vertical Take-Off and Landing (VTOL) aircraft, each with its own set of connatural constraints in terms of flight performance, payload, endurance, maximum high speed, and so on (Saeed et al., 2015). Although VTOLs have their worthy features, performance losses and high consumption values, especially in cruise flights, limit them for fast-speed missions (Dündar et al., 2020). Small fixed-wing conventional UAVs usually cause mission limitations with low cruise speeds and low altitude operations (Çoban, 2019). On the other hand, while the fixed-wing conventional UAVs are more suited to applications requiring long-distance cruise duties, they are generally slow in terms of cruise speed (Khan et al., 2012). These disadvantages of popular small UAVs highlight high-speed UAVs for operations that are necessary to be fast.

Many studies have been carried out on the modeling and control of fixed-wing UAVs. Modeling, simulation, and control design for the longitudinal dynamics of a UAV with a highly stable fixed-wing and dual H-type tail assembly were carried out with USAF DATCOM and X-Plane (Mobarez et al., 2017). In this study, it is determined

that the system responses given by both methods are similar. Aerodynamic analysis, simulation, and flight controller design of a small flying wing UAV were performed for a steady level trim speed of 15 m/s (Wang et al., 2021, Bautista-Medina et al., 2021). To overcome the mortal problem of the linearized model's narrow implementation range, a comprehensive non-linear model of a small battery-powered flying wing UAV was well constituted. In another study (Mekuria et al., 2021), mathematical modeling and designing some controllers of a fixed-wing UAV are evaluated. To avoid singularity in this system, a six-degrees-of-freedom (6DOF) equation of motion was created, and the three rotational angles were constrained. Finally, a non-linear PID control technique is devised for tracking difficulties, airspeed, and attitude control of the vehicle. On the other hand, tilt-wing UAV studies on modeling and control have also been carried out. The mode transition of a new-style dispended propulsion tilt-wing UAV is studied using a multibody attitude dynamics model (Wang et al., 2019). A new finite-time robust controller for altitude dynamics is proposed that can guarantee zero errors in terms of external disturbances while also displaying robustness to force inputs. Furthermore, for the attitude dynamic, a new-based tracking controller is proposed. In a similar study, a dual tilt-wing UAV in vertical flight was developed, modeled, and controlled with a PD-type controller (Sanchez-Rivera et al., 2020). In addition, aerodynamic distortions and vortexes that occur in VTOL aircraft, especially in transitions, have also been studied in detail (Kaya et al., 2021).

Another frequently used technique for controlling mini-UAVs is the Linear Quadratic regulator (LQR) method. In a study, LQR is developed for a fixed-wing UAV during the waypoint search mission, and it is capable of maintaining its trajectory on its own (Ashari et al., 2019, Philips et al., 2002). This LQR controller is accompanied by a proportional gain, increasing the stability of the system. Dharmawan et al. have developed an LQR-based control algorithm for a fixed-wing UAV that can overcome obstacles. Both Proportional Integral Derivative (PID) and LQR control methodologies with a method of integrated action controls were employed to create the lateral and longitudinal control for fixed-wing Micro Aerial Vehicles (MAVs) (Anjali et al., 2016). Results for this study are represented by MATLAB and Simulink, and it is stated that the LQR controller has a higher level of disturbance rejection and overall performance. The optimal control approach is used to create an altitude control system for a mini-UAV with the Kalman filter approach to make the controller more effective (Hajiyev et al., 2013). The simulations show that employing a Kalman filter to predict states' values when there are disturbances improves the LQR controller's performance significantly.

The concept of high-speed UAV is virtually a new term in the aviation literature (Yin et al., 2021). Definition of high-speed UAV is generally used for jet-powered aircraft intended to be used as target UAV (LJ-1, 2019) or supersonic jets (Bougas et al., 2013). Target UAVs are often vehicles with enough space for gasoline and jet engines, as well as a delta wing design that addresses structural difficulties. On the other hand, most fixed-wing electric-powered mini aircraft, which can reach high speeds of about 500 km/h with their small dimensions, are model aircraft used in pylon races (Pylon Racer, 2013).

In this study, the mini-UAV design named Kuzgun is inspired by the fixed-wing electric-powered racing aircraft. Although racing aircraft are not evaluated in the UAV class under normal conditions, in this work, a hybrid design is determined as a research subject that has a general aerodynamic design characteristic of fixed-wing electric-powered racing aircraft with the flight controllers achieving autonomous flight. First, the geometric parameters design of the vehicle is carried out to provide high-speed and low drag. The aerodynamic coefficients and derivations are obtained using Xflr5 and USAF DATCOM with a wide range of flight conditions. Flight simulation studies are implemented with the linearized 6DOF equations of motion by performing thrust, servomotor, atmospheric, gyroscopic, and gravitational modeling. The open-loop system response of the mini-UAV against doublet elevator and rudder inputs with a 5-degree deflection angle is investigated in both longitudinal and lateral directions with the help of a code developed in MATLAB/Simulink. Finally, two different linear controllers, which are PID (Kaba, 2020) and LQR, are designed for mini-UAV, and time-dependent results are compared with elevator effort.

2. Modeling the Mini-UAV

2.1. High-speed Mini-UAV

The aircraft considered in this study is a high-speed fixed-wing electric-powered mini-UAV that is designed to reach high speeds, especially in pull-down maneuvers. The mini-UAV has a 1.2 m long wingspan with a relatively large wing area and high aspect ratio to provide both high-speed and stable flying characteristics with sufficient lift. The MH-30 airfoil, with a thickness of 7.74% and a low drag and moment coefficient, is selected owing to less drag and better performance in terms of maximum speed compared to the similar profiles. It is modified by slightly flattening the base towards the rear so that the total drag and moment coefficient value of the profile is reduced, and it has been made more producible. Modified wing airfoil provides a wide speed range so that the mini-UAV will have a great climb and wind penetration capability affording low drag at high

speeds while maintaining good lift and docile handling at lower speeds.

The increased dihedral angle at the tip of the wing reduces the wing-tip vortices. The wing and the stabilizers are located inline so that the total drag is minimized. The fuselage has a small frontal area and square-like sections to be manufactured easily and to accommodate the large battery and the payload while

decreasing total drag. The maximum take-off weight of the mini-UAV is 1.1 kg with a maximum 200-gram payload. The vertical stabilizer has almost zero taper ratio with enough rudder efficiency to decrease the total drag of the vehicle. High-speed mini-UAVs are comparably listed with some physical and flight characteristics in Table 1. In addition, some geometric specifications with aerodynamic characteristics and a perspective view of high-speed mini-UAV designed are given in Table 2 and Figure 1, respectively.

Table 1. High-speed mini-UAVs

Mini-UAV	Wingspan [mm]	Wing area [m^2]	Aspect ratio	Maximum total weight [g]	Length [mm]	Maximum speed [km/h]
Stinger ARF	950	0.135	6.68	550	760	330
Snipp FG	1300	0.185	9.1	870	725	375
Acro-Prism	1600	0.308	8.3	1250	1100	340
Monster 1.1 SpreadTowsa	1450	0.225	9.34	790	1150	440
Sabre F5B	1710	0.22	13.2	890	1000	390
Kuzgun	1200	0.144	9.98	1100	810	400

The total take-off weight of the mini-UAV, which is designed to have a larger payload volume, is slightly higher than that of other aircraft. The maximum speeds of the investigated vehicles are almost the same with electric power. Apart from this, it is seen that there is a certain ratio between the wingspans and weights of the vehicles.

2.2. 6DOF Equations of Motion

According to (Nicolosi et al., 2013, Padfield, 1996), the twelve equations that make up the non-linear model for fixed-wing aircraft dynamics are based on a body-fixed reference frame. A high-speed fixed-wing mini-UAV can be thought of as a rigid body that moves in three dimensions while being influenced by gravity, aerodynamic, and propulsive forces. As a result, it's a six-degrees-of-freedom (6DOF) system with three translational and three rotational DOF. For such a system, non-linear equations of motion are given in Equation (1).

$$X = m(\dot{u} + qw - rv) \tag{1.1}$$

$$Y = m(\dot{v} + ur - pw) \tag{1.2}$$

$$Z = m(\dot{w} + pv - qu) \tag{1.3}$$

$$L = \dot{p}I_{xx} - I_{xy}(\dot{q} - pr) - I_{xz}(\dot{r} + pq) + (I_{zz} - I_{yy})qr + I_{yz}(r^2 - q^2) \tag{1.4}$$

$$M = \dot{q}I_{yy} - I_{yz}(\dot{r} - pq) - I_{xy}(\dot{p} + qr) + (I_{xx} - I_{zz})pr + I_{xz}(p^2 - r^2) \tag{1.5}$$

$$N = \dot{r}I_{zz} - I_{xz}(\dot{p} - qr) - I_{yz}(\dot{q} + pr) + (I_{yy} - I_{xx})pq + I_{xy}(q^2 - p^2) \tag{1.6}$$

In Equation (1), X, Y, and Z represent total weight, aerodynamic and propulsion forces, L, M and N are the total moments acting on the vehicle, including reaction torque and gyroscopic moments exerted by the thruster on the mini-UAV. Aircraft motion is symbolized by three

translational velocity components, u, v, and w, and three rotational velocity components, p, q, and r, which are called body rates. m represents the mini-UAV's total weight, I_{xx}, I_{yy}, and I_{zz} are moments of inertia, while I_{xy}, I_{yz}, and I_{xz} express the product of inertias. To simplify the non-linear equations of motion, numerous assumptions are applied. The mini-UAV's center of gravity will not have a relative velocity for the body-fixed reference frame because the airframe is presumed to be a rigid body. Second, the mini-UAV mass is assumed to be constant since it is powered with electricity, and finally, mass distribution is assumed to be constant during the flight, resulting in a constant inertia tensor. In addition, equations of motion are typically used in body-fixed axes, earth-fixed frames, and wind axes.
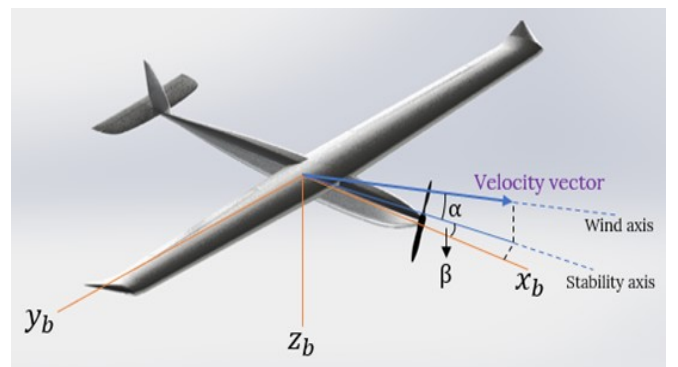

Fig. 1. Fixed-wing high-speed mini-UAV with frames

Obtaining the aerodynamic coefficients is carried out in the wind-axis body frame (Panagiotou et al., 2014). However, all measurement devices are placed on the body-fixed frame to be able to measure the flight characteristics such as velocity and altitude. Therefore,

a relationship and transformation between the different axes on the mini-UAV are inevitable. In other words,

transformation matrices are required to transform

Table 2. Fixed-wing high-speed mini-UAV properties

Wingspan [mm]	Wing area [m²]	Mean aerodynamic chord [mm]	Aspect ratio	Taper ratio	Root-tip sweep angle [°]	Tip twist angle [°]	Dihedral Angle [°]
1200	0.144	124	9.98	0.067	8.34	-1.5	1 at root 10 at tip
Maximum take-off weight [N] 10.79	I_{xx} [kg.m²] 0.036	I_{yy} [kg.m²] 0.0326	I_{zz} [kg.m²] 0.0686	Center of gravity from nose [m] 0.251	Cruise speed [m/s] 43	Maximum speed [m/s] 111	Maximum g-load 2.3
Wing airfoil	Mh-30 modified	Horizontal tail airfoil	NACA 0009	Vertical tail airfoil	NACA 0009	Maximum payload	200 g

between variables stated in the inertial and body frames. The most used kinematic transformation is between body rates and time rates of change of the Euler angles (ϕ ; θ ; and ψ) as given in Equation (2).

$$\begin{pmatrix} \dot{\phi} \\ \dot{\theta} \\ \dot{\psi} \end{pmatrix} = \begin{pmatrix} 1 & tan\theta sin\phi & cos\phi tan\theta \\ 0 & cos\phi & -sin\phi \\ 0 & sec\theta sin\phi & sec\theta cos\phi \end{pmatrix} \begin{pmatrix} p \\ q \\ r \end{pmatrix} \quad (2)$$

Another widely used conversion is from earth-fixed frame to wind-axis frame as given in Equation (3). $\dot{x}$; $\dot{y}$; and $\dot{z}$ represent the trajectory directions.

2.3. Aerodynamic Modeling

Estimating the aerodynamic coefficients and derivatives is the most severe and, at the same time, the most crucial part. Aerodynamic coefficients and derivatives are assigned as inputs to 6DOF simulations as well as for the designed controllers. In addition, different flow

conditions can cause significant changes in the coefficient and its derivatives. The aerodynamic coefficients can be explained in different methods. However, in this study, a basic but logical formula (Gryte et al., 2018) is performed, as shown in Equation (4) and Equation (5).

Where α and β show the angle of attack, the sideslip angle, δ_e, δ_a, and δ_r represent the elevator, aileron, and rudder deflection angles, respectively. In addition, C_L, C_D, and C_Y are the lift, drag, and side force coefficients, respectively. C_l, C_m, and C_n refer to the aerodynamic moments along the x, y, and z-axis of the body-fixed-frame, respectively. All the aerodynamic coefficients are calculated in compliance with the given equations through Xflr5 and USAF DATCOM and are represented in Table 3. The ungiven coefficients are neglected.

$$\begin{pmatrix} \dot{x} \\ \dot{y} \\ \dot{z} \end{pmatrix} = \begin{pmatrix} cos\psi cos\theta & cos\psi sin\theta sin\phi - sin\psi cos\phi & cos\psi sin\theta cos\phi + sin\psi sin\phi \\ sin\psi cos\theta & sin\psi sin\theta sin\phi + cos\psi cos\phi & sin\psi sin\theta cos\phi - sin\psi sin\phi \\ -sin\theta & cos\theta sin\phi & cos\theta cos\phi \end{pmatrix} \begin{pmatrix} u \\ v \\ w \end{pmatrix} \quad (3)$$

$$\begin{bmatrix} C_L \\ C_D \\ C_Y \end{bmatrix} = \begin{bmatrix} C_{L_0} + C_{L_\alpha}\alpha + C_{L_q}(c/2V)q + C_{L_{\delta_e}}\delta_e \\ C_{D_0} + C_{D_\alpha}\alpha + C_{D_{\delta_e}}\delta_e + C_{D_\beta}\beta + C_{D_q}(c/2V)q \\ C_{Y_0} + C_{Y_\beta}\beta + C_{Y_p}(b/2V)p + C_{Y_r}(b/2V)r + C_{Y_{\delta_a}}\delta_a + C_{Y_{\delta_r}}\delta_r \end{bmatrix} \quad (4)$$

$$\begin{bmatrix} C_l \\ C_m \\ C_n \end{bmatrix} = \begin{bmatrix} C_{l_0} + C_{l_\beta}\beta + C_{l_p}(b/2V)p + C_{l_r}(b/2V)r + C_{l_{\delta_a}}\delta_a + C_{l_{\delta_r}}\delta_r \\ C_{m_0} + C_{m_\alpha}\alpha + C_{m_{\delta_e}}\delta_e + C_{m_q}(c/2V)q \\ C_{n_0} + C_{n_\beta}\beta + C_{n_p}(b/2V)p + C_{n_r}(b/2V)r + C_{n_{\delta_a}}\delta_a + C_{n_{\delta_r}}\delta_r \end{bmatrix} \quad (5)$$

Table 3. Aerodynamic coefficients and derivatives

Coefficient	Value	Coefficient	Value	Coefficient	Value	Coefficient	Value
C_{L_0}	0.177	C_{D_q}	0	C_{l_β}	-0.13	$C_{m_{\delta_e}}$	-0.99
C_{L_α}	5.61	C_{Y_0}	0	C_{l_p}	-0.51	C_{m_q}	-38.21
$C_{L_{\delta_e}}$	0.13	C_{Y_β}	-0.83	C_{l_r}	0.25	C_{n_β}	0.073
C_{D_0}	0.023	C_{Y_p}	0	$C_{l_{\delta_a}}$	0.17	C_{n_p}	-0.069
C_{D_α}	0.027	C_{Y_r}	-0.013	$C_{l_{\delta_r}}$	0.0024	C_{n_r}	-0.095
$C_{D_{\delta_e}}$	0.0135	$C_{Y_{\delta_a}}$	0.075	C_{m_0}	0.0135	$C_{n_{\delta_a}}$	-0.011
C_{D_β}	0.037	$C_{Y_{\delta_r}}$	0.19	C_{m_α}	-2.74	$C_{n_{\delta_r}}$	-0.068

2.4. Propulsion Modeling

The propulsion system of a fixed-wing UAV is composed of a propeller, brushless DC (Direct Current) motor, battery (Lithium Polymer or Lithium-Ion), and ESC (Electronic Speed Control). Since the mini-UAV has high speeds TP3640 7D-KV2080-4 brushless motor is selected with 3000 mAh 6S1P 22.2V Li-Po, 150A ESC, and 12x8 propeller.

The thrust of the high-speed mini-UAV is accepted to be composed of motor/propeller pair. The inputs to the thrust model will be the airspeed of the aircraft V and the throttle setting. It is accepted that the thrust and moment vectors produced by the propeller/motor pair are aligned with the rotation axes of the motor and are denoted by the magnitude of the thrust is T. The standard model for the thrust produced by a propeller is given by propeller theory (Mahmuddina, 2017) as Equation (6).

$$T = (\rho D^4/4\pi^2)\Omega C_T \tag{6}$$

where D is the diameter of the propeller, Ω is the propeller speed in radians per second, and C_T represents the thrust coefficient which is found from literature data. It is also assumed that the input voltage (V_{in}) of the battery is a linear function of the throttle level. Therefore, Equation (7) can be derived.

$$V_{in} = V_{max}\delta_t \tag{7}$$

When a DC motor drives the propeller, torques around the propeller and motor can be assumed as equal (Emhemed et al., 2012).

$$(\rho D^5/4\pi^2)C_{Q_0}\Omega^2 + (\rho D^4/2\pi C_{Q_1}V + (K_Q{}^2/R))\Omega + \rho D^3 C_{Q_2}V^2 - (K_Q/R)V_{in} + K_Q i_0 = 0 \tag{8}$$

where C_Q is a non-dimensional aerodynamic coefficient, K_Q is the motor torque constant, R is the resistance of the motor windings, i_0 is the no-load current. From Equation (8) operating speed of the propeller Ω can be calculated numerically.

2.5. Servomotor Modeling

The mini-UAV is fitted with two DC servo motors that control the aileron and elevator deflection. The servo motors' reaction characteristics will have a direct impact on the UAV's attitude control, so servo motor modeling is crucial. A second-order system technique (Sufendi et al., 2013) is utilized to model the servo motor. Equation (9) depicts the servo motor's transfer function with the classical notation method.

$$\frac{Y(s)}{X(s)} = \frac{95.53}{s^2 + 15.65s + 95.53} \tag{9}$$

2.6. Atmospheric Modeling

The atmospheric sub-system returns density, temperature, pressure, dynamic and kinematic viscosity, speed of sound, and gravitation acceleration whereas the input is just altitude. In atmospheric modeling, the atmosphere is assumed to be steady and does not change with time (Daidzic, 2015).

2.7. Gyroscopic Modeling

Rotating rigid bodies have angular momentum and if an external moment acts on the rigid body that generates angular velocity, gyroscopic moments are generated to conserve previous angular momentum by producing a counter moment which is called the gyroscopic precession effect. The gyroscopic moment of the center of gravity can be calculated as given in Equation (10) where ω is the angular rate of the aircraft and H_P represents the transformation matrix from the propulsion reference frame to the body-fixed frame. x, y, and z subscripts denote the directions where the moments act on. Besides, i_B, j_B, and k_B represent unit vectors in the body frame.

$$\sum M_{Gy} = -dH_P/dt - \omega \times H_P = -\begin{pmatrix} (qH_{P,z} - rH_{P,y})i_B \\ (rH_{P,x} - pH_{P,z})j_B \\ (pH_{P,y} - qH_{P,x})k_B \end{pmatrix} \tag{10}$$

2.8. Gravitational Modeling

Gravitational force is calculated as given in Equation (11) due to the gravitation. F_G represents the gravitational force θ, and ϕ shows the orientation of the aircraft with respect to the reference frame, which is the earth's fixed-frame

$$F_G = \begin{pmatrix} -mg\,sin\theta \\ mg\,cos\theta\,sin\phi \\ mg\,cos\theta\,cos\phi \end{pmatrix} \tag{11}$$

2.9. Linearization of Non-linear Equations of Motion

Due to the need for accurate representations of the intricate vehicle dynamics, analyzing the stability of a non-linear system is challenging and time-consuming. In addition, since fixed-wing aircraft are linear in most of their flight by nature, it is quite reasonable to linearize the non-linear equations according to the Small Disturbance Theory (Philips et al., 2002) for the steady level flight trim condition. Besides, linear systems enable the use of linear controllers, which are a more straightforward and cost-effective method of developing controllers for fixed-wing UAVs. Linearized equations of motion around the steady, wings-level, trimmed flight of fixed-wing mini-UAV are given in Equation (12).

$$\Delta X = m(\dot{u} - Wq + (g\cos\theta_0)\theta) \tag{12.1}$$

$$\Delta Y = m(\dot{v} + Vr - Wp - (g\cos\theta_0)\phi) \tag{12.2}$$

$$\Delta Z = m(\dot{w} - Vq + (g\cos\theta_0)\theta) \tag{12.3}$$

$$\Delta L = I_{xx}\dot{p} - I_{xz}\dot{r} \tag{12.4}$$

$$\Delta M = I_{yy}\dot{q} \tag{12.5}$$

$$\Delta N = I_{zz}\dot{r} - I_{xz}\dot{p} \qquad\qquad (12.6)$$

where V is forward speed, W is the total weight, θ_0 is the unperturbed flight path angle. While deriving these equations, it is assumed that angular velocities are zero, and some stability derivatives don't affect the steady level flight.

Modeling the high-speed fixed-wing mini-UAV with all circumstances, Figure 2 and Figure 3 represents the open-loop 6DOF simulation results for 155 km/h steady level trimmed flight which is developed by MATLAB/Simulink environment for longitudinal and lateral planes, respectively.

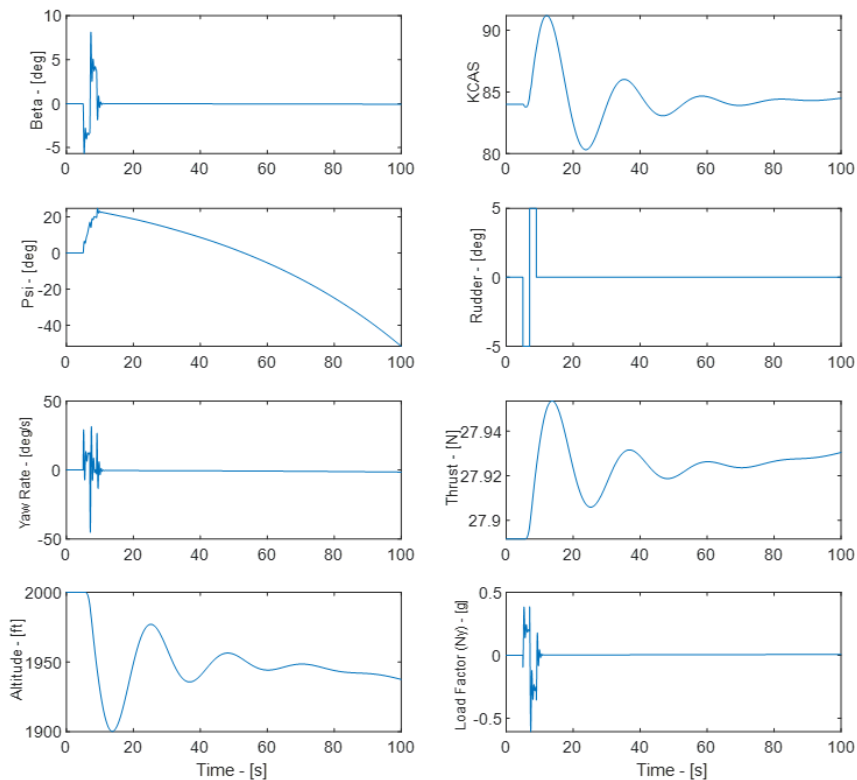**Fig. 2**. Longitudinal open-loop 6DOF simulation results in Simulink

Fig. 3. Lateral open-loop 6DOF simulation results in Simulink

In the 100-second flight simulation, -5 and +5 degrees of doublet input are entered into the elevator and rudder at the 5th second of the flight, and the response of the mini-UAV is examined. The mini-UAV is inherently stable in all flight modes in the longitudinal direction, and its response to elevator disturbance causes a 10% fluctuation in altitude and speed. In the lateral direction, the vehicle is unstable only for spiral mode; this is due to the positive pole in the right half of the s-plane, which is +0.0164. For a highly maneuverable and high-speed mini-UAV, this instability in spiral mode can be easily tolerated (Yanık et al., 2014). The details of the longitudinal and lateral flight modes of the high-speed mini-UAV are presented in Table 4.

Table 4. Longitudinal and lateral flight modes properties

Short-period frequency [rad/s]	Short-period damping	Phugoid frequency [rad/s]	Phugoid damping	Dutch roll frequency [rad/s]	Dutch Roll Damping	Spiral Stability time to double [s]	Roll Mode time to half [s]
15.98	0.487	0.277	0.204	9.68	0.223	42.45	0.019

$$\begin{bmatrix} \Delta \dot{V}_T \\ \Delta \dot{\alpha} \\ \Delta \dot{q} \\ \Delta \dot{\theta} \end{bmatrix} = \begin{bmatrix} -5.7462 & 0.0725 & -3.0927 & 0 \\ -0.6821 & -0.0724 & 0.4032 & -9.8104 \\ 30.052 & -0.5229 & -5.0221 & -0.2225 \\ 1 & 0 & 0 & 0 \end{bmatrix} \begin{bmatrix} \Delta V_T \\ \Delta \alpha \\ \Delta q \\ \Delta \theta \end{bmatrix} + \begin{bmatrix} -0.8504 \\ -0.0050 \\ -0.0620 \\ 0 \end{bmatrix} \Delta \delta_e \qquad (13)$$

3. Controller Design for Pitch Angle

The equations of motion are split into longitudinal motion, which includes variables V, α, q, θ, and lateral motion, which includes states β, ϕ, ψ, p, r, after linearization. The Linear state-space model of longitudinal and lateral dynamics is given in Equation (13). On the other hand, the effect of the throttle has been removed since linearization is done in an equilibrium flight condition where the thrust force is constant.

3.1. PID Controller

To keep the altitude constant, the PID controller design of the high-speed mini-UAV is carried out first. The elevator deflection angle versus the pitch angle transfer function is obtained as given in Equation (14). This transfer function has been tuned in the Simulink environment with the servo model transfer function given in section 3.3, and the controller design has been realized. The response of the PID controller for the reference angle of 30 degrees pitch angle and the effort of the elevator for this response are presented in Figure 4.

$$\frac{\theta(s)}{\delta_e(s)} = \frac{-48.73s^3 - 237.3s^2 - 27.86s}{s^4 + 10.84s^3 + 122.8s^2 + 10.52s + 19.38} \qquad (14)$$

3.2. LQR-I Controller

LQR is a well-known approach for creating closed-loop stable and high-performance systems by providing appropriately managed feedback gains. The objective function J is minimized with the formation of the controller K. A feedback gain matrix is built in this technique to minimize the objective function J and establish a balance between the usage of the size, the speed of response, and the control exertion, resulting in a stable system.

$$J = \int_0^\infty (x^T Q x + u^T R u) dt \qquad (15)$$

where Q and R are the weight matrices that must be a positive definite or positive semi-definite symmetry matrix. In order to minimize the cost function value, the controller K is calculated according to Equation (16)

$$K = R^{-1} B^T P \qquad (16)$$

In Equation (15) P is calculated by solving the Algebraic Ricatti Equation (ARE) (Petersen et al., 1986). In addition, an integrator is added to the system to be able to procure zero steady-state error. The LQR-I controller design can be formulated as follows:

- Estimation of the matrices Q and R

- Calculation of P from ARE

- Finding the state feedback matrix K using $K = R^{-1} B^T P$

The response of the LQR-I controller for the reference angle of 30 degrees pitch angle and the effort of the elevator for this response are given in Figure 4. A challenging task for reference theta is given as input to the system, and the responses of the controllers are evaluated in Figure 5. The PID controller can successfully follow the desired reference value with a little overshoot. LQR-I controller, on the other hand, could not follow the reference value and left a steady-state error.
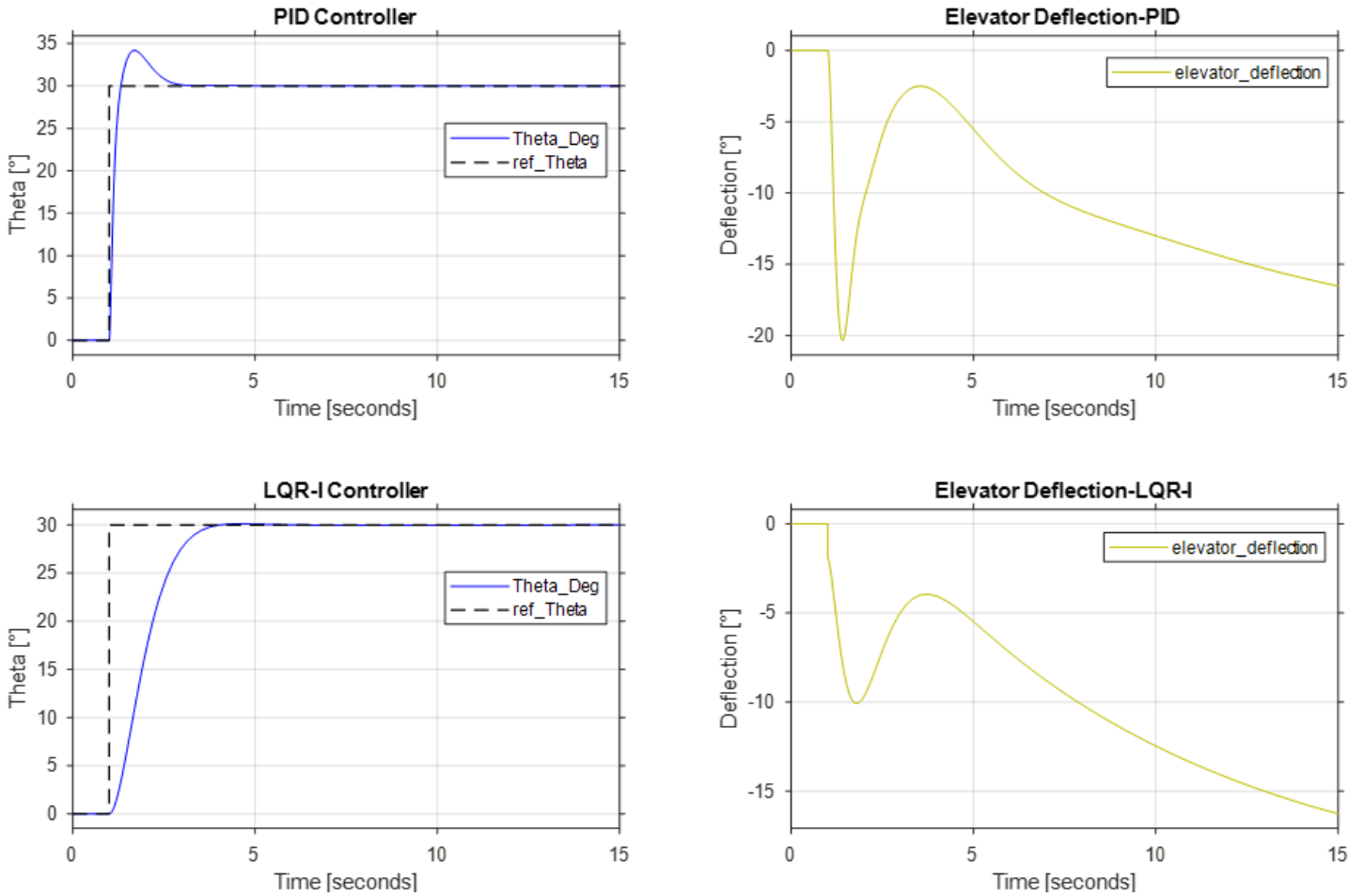
Fig. 4. Pitch angle control with PID and LQR-I controllers and corresponding elevator efforts
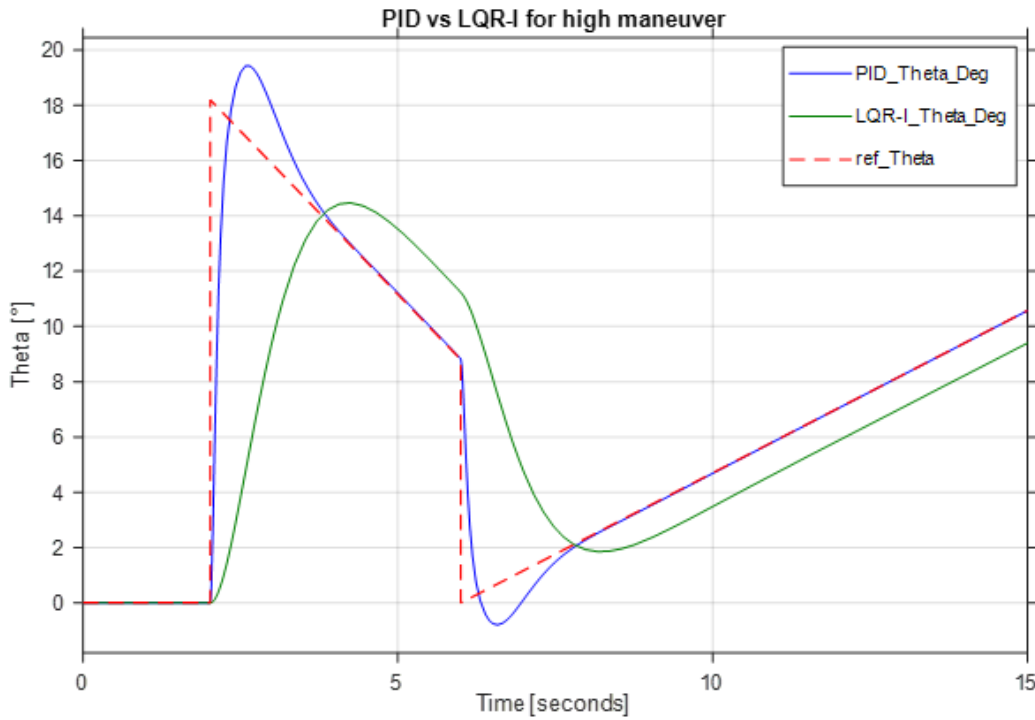

Fig. 5. PID vs LQR-I responses to a compulsive theta reference angle

4. Conclusion

In this study, 6DOF flight simulation studies and two different controller designs are carried out for a fixed-wing high-speed mini-UAV. Unlike standard fixed-wing UAVs, the high-speed mini-UAV can reach a speed of 400 km/h, especially in pull-down maneuvers, and has a

conventional design with a wingspan of 1.2 meters and a total take-off weight of 1.1 kg. The aerodynamic analysis of the mini-UAV and the derivation of its coefficients are obtained with Xflr5 and USAF DATCOM. Aerodynamic, propulsion, servomotor, gyroscopic, atmospheric, and gravitational modeling is performed under suitable conditions. 6DOF flight simulation studies are implemented with a code developed in MATLAB/Simulink environment. The simulation features and results suggest that:

- The mini-UAV is trimmed at 155 km/h wing-level, steady flight.

- The mini-UAV responses as statically and dynamically stable to the doublet elevator and rudder deflection angles.

- Load factor (n) exceeds the 2-g after the elevator disturbance

- Altitude and speed changes are observed slightly low after the control surface deflections.

- The mini-UAV is unstable for only the spiral flight mode in the lateral direction.

- Since the spiral mode requires long flight times, the pole placement method is not addressed to eliminate this instability

Both longitudinal and lateral transfer functions are obtained by considering the trim conditions in the 6DOF simulation studies. Two controllers are designed for high-speed mini-UAV using PID and LQR-I methods using these transfer functions. The main conclusions from the controller designs are:

- The PID controller responded to the reference theta angle of 30 degrees faster than the LQR-I controller.

- The PID controller has an overshoot and its settling time is shorter than the LQR-I controller. This situation caused the vehicle to respond faster to the reference value.

- LQR-I controller gives a smoother and late response without overshoot compared to PID.

- Elevator efficiency is good enough for both controllers to hold the theta angle in the desired value.

- For compulsory reference theta input, the PID controller can successfully follow the target reference value with a little overshoot.

- The LQR-I controller is unable to track the reference value and hence produces a steady-state error under the same compulsory reference theta input.

In conclusion, the PID controller results in a high-performance response with some overshoot, while the LQR-I controller imparts a low-performance response with high stability. In future work, a robust controller will be designed for the high-speed fixed-wing mini-UAV.

Abbreviations

UAV	:	Unmanned Aerial Vehicle
PID	:	Proportional Integral Derivative
LQR-I	:	Linear Quadratic Regulator with Integral
VTOL	:	Vertical Take-off Landing
6DOF	:	Six Degree of Freedom
DC	:	Direct Current
ESC	:	Electric Speed Control
CFD	:	Computational Fluid Dynamics

CRediT Author Statement

Mesut Bilici: Conceptualization, Methodology, Software, Investigation, Validation, Writing-Original Draft, Visualization. **Mehmet Karalı:** Resources, Data Curation, Supervision, Project administration.

References

Anjali, B. S., Vivek, A., & Nandagopal, J. L. (2016). Simulation and Analysis of Integral LQR Controller for Inner Control Loop Design of a Fixed Wing Micro Aerial Vehicle (MAV). Procedia Technology, (25), 76-83.

Ashari, A., Dharmawan, A., Fadhli, & H., Handayani, A. (2019). Flight Trajectory Control System on Fixed Wing UAV using Linear Quadratic Regulator. International Journal of Engineering Research & Technology (IJERT), 8(8), 2278-0181.

Bautista-Medina, J. A., Lozano, R., & Osorio-Cordero, A. (2021). Modeling and Control of a Single Rotor Composed of Two Fixed Wing Airplanes. Drones, 5(3), 92.

Bougas, L., & Hornung, M. (2013). Propulsion system integration and thrust vectoring aspects for scaled jet UAVs. CEAS Aeronautical Journal, 4(3), 327-343.

Çoban, S. (2019). Different Autopilot Systems Design for a Small Fixed Wing Unmanned Aerial Vehicle. Avrupa Bilim ve Teknoloji Dergisi, (17), 682-691.

Daidzic, N. E. (2015). Mathematical Model of Hot-Air Balloon Steady-State Vertical Flight Performance. Aviation, 25(3), 149-158.

Dharmawan, A., Putra, A. E., Tresnayana, M., & Wicaksono W. A. (2019, January). The Obstacle Avoidance System in A Fixed-Wing UAV When Flying Low Using LQR Method. In International Conference on Computer Engineering Network,

and Intelligent Multimedia (CENIM) (pp. 1-7

Dündar, Ö., Bilici, M., & Ünler, T. (2020). Design and performance analyses of a fixed wing battery VTOL UAV. Engineering Science and Technology, an International Journal, 23(5), 1182-1193.

Emhemed, A. A., & Mamat, R. B. (2012). Modelling and Simulation for Industrial DC Motor Using Intelligent Control. Procedia Engineering, 41, 420-425.

Gryte, K., Hann, R., Alam, M., Rohac, J., Johansen, T.A., & Fossen, T.I. (2018). Aerodynamic modeling of the Skywalker X8 Fixed-Wing Unmanned Aerial Vehicle. In Proceedings of the International Conference on Unmanned Aircraft Systems (ICUAS), (pp. 826–835).

Hajiyev, C., & Vural, S. Y. (2013). LQR Controller with Kalman Estimator Applied to UAV Longitudinal Dynamics. Positioning, 4(1), 36-41.

Kaba, A. (2020). A Comparative Study on the Tuning of the PID Flight Controllers Using Swarm Intelligence. International Journal of Aviation Science and Technology, 1(2), 80-91.

Kaya, M. N., Kok, A. R., & Kurt, H. (2021). Comparison of aerodynamic performances of various airfoils from different airfoil families using CFD. Wind and Structures, 32(3), 239-248.

Khan, W., & Nahon, M. (2015, June). Real-time modeling of agile fixed-wing UAV aerodynamics. In International Conference on Unmanned Aircraft Systems (ICUAS) (pp. 1188-1195).

LJ-1 (Target Drone), Available at: https://www.militarydrones.org.cn/lj-1-high-speed-target-drone-p00452p1.html, (accessed 1 March 2022)

Mahmuddina, F. (2017). Rotor Blade Performance Analysis with Blade Element Momentum Theory. Energy Procedia, 105(2017), 1123-1129.

Mekuria, S., Belete, M., & Niguse, B. (2021). Fixed Wing Unmanned Aerial Vehicle Control by Using a Non-linear PID Controller. Journal of Electrical Engineering, Electronics, Control and Computer Science, 7(24), 39-46.

Nicolosi, F., Vecchia, P. D., & Ciliberti, D. (2013). An investigation on vertical tailplane contribution to aircraft sideforce. Aerospace Science and Technology, 28(1), 401-416.

Yanık, N. S., Özyetiş, E., Güçlü, Ö., Kayran, A., Kıran, E., & Alemdaroğlu, N. (2014, May). Design and manufacturing of a high-speed jet powered UAV. In International Conference on Unmanned Aircraft Systems (ICUAS) (pp. 1073-1080).

Padfield, G., Helicopter Flight Dynamics (1996): The Theory and Application of Flying Qualities and Simulation Modeling. American Institute of Aeronautics and Astronautics.

Panagiotou, P., Kaparos, P., & Yakinthos, K. (2014). Winglet design and optimization for a MALE UAV using CFD. Aerospace Science and Technology, 39(2014), 190-205.

Petersen, I. R., & Hollot, C. V. (1986). A riccati equation approach to the stabilization of uncertain linear systems. Automatica, 22(4), 397-411.

Philips, W. F., & Santana, B. W. (2002). Aircraft Small-Disturbance Theory with Longitudinal&Lateral Coupling. Journal of Aircraft, 39(6), 973-980.

Pylon Racer (Racing aircrafts), Available at: https://icare-icarus.3dcartstores.com/Pylon-Racer-F5D_c_28.html, (accessed 1 March 2022)

Saeed, A., Younes, A. B., Islam, S., Dias, J., Seneviratne, L., & Cai, G. (2015, June). A review on the platform design, dynamic modeling, and control of hybrid UAVs. In International Conference on Unmanned Aircraft Systems (ICUAS) (pp. 806-815).

Sanchez-Rivera, L. M., Lozano, R., & Arias-Montano, A. (2020). Development, Modeling and Control of a Dual Tilt-Wing UAV in Vertical Flight. Drones, 4(4), 71.

Mobarez, E. N., Sarhan, A., & Ashry, M. M. (2019). Modeling of fixed wing UAV and design of multivariable flight controller using PID tuned by local optimal control. In IOP Conference Series: Materials Science and Engineering 610 (2019) 012016.

Sufendi, Trilaksono, B.R., Nasution, S.H., & Purwanto, E.B. (2013). Design and implementation of hardware-in-the-loop-simulation for UAV using PID control method. In Proceedings of the 3rd International Conference on Instrumentation, Communications, Information Technology, and Biomedical Engineering (pp. 124–130).

Wang, Y., Zhu, H., Zhao, Z., Zhang, C., & Lan, Y. (2021). Modeling, System Measurements and Controller Investigation of a Small Battery-Powered Fixed-Wing UAV. Machines, 9(12), 333.

Wang, Y., Zhou, Y., & Lin, C. (2019). Modeling and control for the mode transition of a novel tilt-wing UAV. Aerospace Science and Technology, 91(2019), 593-606.

Yin, Q., Wei, X., Nie, H., & Deng, J. (2021). Parameter effects on high-speed UAV ground directional stability using bifurcation analysis. Chinese Journal of Aeronautics, 34(11), 1-14.